Amplitude equation and pattern selection in Faraday waves

Peilong Chen[1] and Jorge Viñals[1,2]
[1]*Supercomputer Computations Research Institute, Florida State University, Tallahassee, Florida 32306-4130*
[2]*Department of Chemical Engineering, FAMU-FSU College of Engineering, Tallahassee, Florida 31310-6046*
(Received 7 January 1999)

A nonlinear theory of pattern selection in parametric surface waves (Faraday waves) is presented that is not restricted to small viscous dissipation. By using a multiple scale asymptotic expansion near threshold, a standing wave amplitude equation is derived from the governing equations. The amplitude equation is of gradient form, and the coefficients of the associated Lyapunov function are computed for regular patterns of various symmetries as a function of a viscous damping parameter γ. For $\gamma \sim 1$, the selected wave pattern comprises a single standing wave (stripe pattern). For $\gamma \ll 1$, patterns of square symmetry are obtained in the capillary regime (large frequencies). At lower frequencies (the mixed gravity-capillary regime), a sequence of sixfold (hexagonal), eightfold, ... patterns are predicted. For even lower frequencies (gravity waves) a stripe pattern is again selected. Our predictions of the stability regions of the various patterns are in quantitative agreement with recent experiments conducted in large aspect ratio systems. [S1063-651X(99)08607-9]

PACS number(s): 47.20.Ky, 47.35.+i, 47.54.+r

I. INTRODUCTION

This paper extends an earlier calculation by Zhang and Viñals of the amplitude equation governing Faraday waves in the weakly nonlinear regime [1]. In order to make the problem analytically tractable, they neglected without rigorous justification viscous terms in the boundary conditions at the free fluid surface that had a nonlinear dependence on either the surface displacement away from planarity, or on the surface velocity. Even though the resulting amplitude equation led to the prediction of stationary patterns that are generally in agreement with experiments conducted in the regime of weak viscous dissipation [2,3], the unsystematic nature of the truncation makes it difficult to assess the range of validity of the theory. In particular, the so-called stripe pattern (a pattern comprised of a single standing wave), which is generically observed when viscous dissipation is not small, could not be obtained in their analysis for any range of parameters. We extend below this earlier work, and present a systematic weakly nonlinear theory of Faraday waves. Our results on pattern selection agree with those of Zhang and Viñals [4,1] in the limit of small viscous dissipation, and with recent experimental work otherwise. A brief summary of our results has already been given in Ref. [5].

Parametrically driven surface waves (also known as Faraday waves) can be excited on the free surface of a fluid layer that is periodically vibrated in the direction normal to the surface at rest when the amplitude of the driving acceleration is large enough to overcome the dissipative effect of fluid viscosity [6,7]. Of special concern to us is the issue of pattern selection in a layer of lateral dimension much larger than the excited wavelength (see, e.g., [8] for a recent review on pattern formation). In the case of Faraday waves, it is now known that different wave patterns can be excited depending on the fluid properties and the driving amplitude or frequency. At high viscous dissipation (a fluid of large viscosity and/or a low driving frequency), the observed wave pattern above threshold consists of parallel stripes [9,10]. For lower dissipation, patterns of square symmetry (combinations of two perpendicular plane waves) are observed in the capillary regime (large frequencies) [11–14], [15,16,9]. At lower frequencies (the mixed gravity-capillary regime), higher symmetry patterns have been observed: hexagonal [17,2], and hexagonal, eightfold, and tenfold [3]. The aim of this paper is to present a weakly nonlinear analysis of Faraday waves that predicts stationary wave patterns with these symmetries.

The derivation of an amplitude equation is a classical method to describe excited states beyond linear instability. Just above threshold, the evolution of the system is assumed to be described in terms of the complex amplitude A of the most unstable mode according to linear theory. The equation of motion for A is often of the form

$$\frac{dA}{dt} = \alpha A - gA^3, \tag{1}$$

where α is the linear growth rate, and $g>0$ is real. The low order nonlinear term provides saturation. There exist cases, however, in which spatial isotropy permits waves to be excited in any direction, and the nonlinear interaction term in the equation above contains terms of the form $g_{ij}|A_j|^2 A_i$, with A_i and A_j the slowly varying amplitudes of two degenerate unstable modes. If the coupling coefficients g_{ij} are known, the resulting wave pattern can be predicted from Eq. (1), as has been illustrated in Ref. [18] for Faraday waves.

The derivation of amplitude equations for surface waves is greatly simplified in the case of an ideal (inviscid) fluid. Since the bulk flow is irrotational, there exists a Hamiltonian formulation in which the canonically conjugate variables are the surface displacement and the velocity potential at the free surface [19,20]. As a consequence, early analyses of Faraday waves were based on the Hamiltonian description of the inviscid limit, and treated viscous or dissipative effects as a perturbation [21–23]. The derivation usually starts from the set of ideal fluid equations [24], written in terms of the velocity potential ϕ. The linear or zeroth order solution ϕ_0 is a

sum over waves of frequency ω and wave vector $\{\mathbf{k}_j\}$, with ω and $k=\|\mathbf{k}_j\|$ related by the ideal fluid dispersion relation [Eq. (15) below]:

$$\phi_0=\frac{-i\omega}{k}e^{kz}\sum_j A_j(T)e^{i(\mathbf{k}_j\cdot\mathbf{x}-\omega t)}+\text{c.c.},$$

where $T=\epsilon t$ is a slow time scale, with $\epsilon\ll 1$ the dimensionless distance away from threshold. An expansion of the ideal fluid equations to third order in ϵ yields the equation for $A_j(T)$ [22],

$$\frac{dA_j}{dT}=-\frac{ikf}{4\omega}A^*_{-j}+i\sum_k \Pi^{(1)}_{jk}|A_k|^2A_j+i\sum_k \Pi^{(2)}_{jk}A_kA_{-k}A^*_{-j}, \tag{2}$$

with f the amplitude of the driving acceleration, and Π *real* functions of the angle between the jth and kth wave vectors. The fact that the coefficients of the cubic terms are purely imaginary follows from the requirement that Eq. (2) be invariant under time reversal as is appropriate for a purely Hamiltonian or reversible system [8,25]. Furthermore, these cubic terms do not contribute to wave saturation in the standing wave equation that follows near threshold [22].

In the limit of small viscous dissipation, Hamilton's equations have been supplemented with a dissipation function [21–23], which is computed under the assumption that the dominant contribution to viscous dissipation arises from the irrotational velocity field in the bulk, and not from friction at the container walls or dissipation near the free surface. Under this assumption, the rate of energy loss is given by [26]

$$\dot{E}=-2\eta\int dV\left(\frac{\partial^2\phi}{\partial x_i\,\partial x_j}\right)^2,$$

where η is the shear viscosity, and the integral extends over the bulk fluid. The velocity potential ϕ is now expanded in powers of ϵ, and viscous contributions computed order by order in ϵ. This procedure leads to real components of the coefficients of the cubic terms in Eq. (2), and to wave saturation. The precise functional form of the coefficients obtained by this method is still somewhat controversial [23,27].

The central contribution to pattern selection in Faraday waves arises from triad resonant interactions. Since the standing wave amplitude equation must be invariant under $A_j\rightarrow -A_j$, it does not contain quadratic terms [28]. Triad resonance can, however, contribute significantly to the coefficients of the cubic order term through the coupling between the zeroth order unstable and first order stable waves. This resonance was already encountered by Milner as a divergence of the cubic coefficient in the standing wave amplitude equation at a particular angle [22]. Later, Edwards and Fauve [9] suggested that triad resonance would be important at low viscous dissipation, a range in which linearly stable modes are only weakly damped. Such a contribution was later computed explicitly [1], and it was shown that it is important in determining the symmetry of the selected pattern in the region of small γ. In particular, a sequence of quasiperiodic patterns was predicted in the region in which the resonant angle approaches zero. As we argue below, dissipation through excitation of resonant stable waves is dominant at low damping, and is an important contribution to the cubic coefficients of the standing wave amplitude equation in this limit. The explicit incorporation of this contribution is the main difference between the approach presented in this paper and earlier theoretical work based on the inviscid limit solution.

We also address the effect of the rotational component of the flow. The dimensionless group involving the ratio of viscous to inertial effects is the damping parameter $\gamma=2\nu k_0^2/\omega_0$, where k_0 is the critical wave number in the inviscid limit, and ω_0 its angular frequency (γ is inversely proportional to the Reynolds number of the flow). An expansion of the governing equations and boundary conditions in powers of γ shows that in the weak dissipation limit, the dominant terms in the boundary conditions are $O(\gamma)$, with a first correction at $O(\gamma^{3/2})$ [29]. At *linear* order in the surface displacement or surface velocity, terms of $O(\gamma)$ are purely irrotational, while the rotational flow component contributes at $O(\gamma^{3/2})$. This result is consistent with a recent linear stability analysis of Faraday waves [30] (see also Sec. II). The dimensionless value of the driving amplitude at threshold equals γ, with a first correction term that is proportional to $\gamma^{3/2}$. The dominant contribution arises solely from the irrotational flow component, with contributions from the rotational component coming at $O(\gamma^{3/2})$. However, we argued that the lowest order contributions to the cubic order coefficients of the amplitude equation are of $O(\gamma)$ for both irrotational and rotational components [1]. Hence rotational flow cannot be neglected in a nonlinear theory, even in the limit of small dissipation. For example, the kinematic boundary condition at the free surface does include one such term proportional to γ that arises from the component normal to the surface of the rotational part of the velocity field. This term was retained both in the analysis of Ref. [1], and in our analysis below, but not in previous approaches based on a dissipation function.

We extend in this paper the analysis of Zhang and Viñals [1] that was based on a quasipotential approximation to the governing equations. By separating the rotational flow within a small vortical layer near the free surface from the potential flow in the bulk, they derived a standing wave amplitude equation valid in the limit of small viscous dissipation. The calculation, however, relied on an uncontrolled approximation concerning nonlinear viscous terms and, as a consequence, its region of validity is difficult to assess. We describe below a systematic expansion of the Navier-Stokes equation and boundary conditions that overcomes this difficulty and that leads to an amplitude equation not restricted to small viscous dissipation. Following the earlier formulation of Kumar and Tuckerman [31,32], we start by deriving an implicit relation for the threshold of instability, which is then used in the nonlinear analysis. The result that we obtain agrees with a recent low viscosity approximation to the governing equations [30]. We then use a multiple scale expansion to derive a standing wave equation which is of gradient form. Minimization of the associated Lyapunov function leads to the prediction of stationary patterns of different symmetries as a function of the fluid parameters and frequency of the driving acceleration. Our predictions are in good agreement with experiments conducted in large aspect ratio cells.

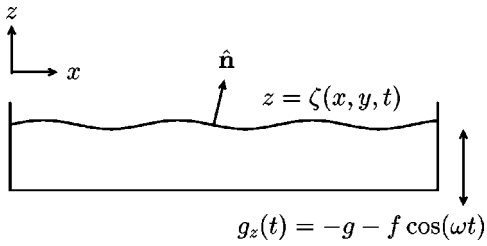

FIG. 1. Schematic setup of a Faraday wave configuration.

II. GOVERNING EQUATIONS AND LINEAR STABILITY

We consider a semi-infinite fluid layer, unbounded in the x-y direction, extending to $z=-\infty$, and with a planar free surface at $z=0$ when at rest. The fluid is assumed incompressible and Newtonian. Under periodic vibration of the layer in the direction normal to the surface at rest, the equation governing fluid motion (in the comoving reference frame) is

$$\partial_t \mathbf{u}+(\mathbf{u}\cdot\boldsymbol{\nabla})\mathbf{u}=-\frac{1}{\rho}\boldsymbol{\nabla}p+\nu\nabla^2\mathbf{u}+g_z(t)\hat{\mathbf{e}}_z, \tag{3}$$

with $\mathbf{u}$ the velocity field, p the pressure, ρ and ν the density and kinematic viscosity of the fluid, respectively, and $g_z(t)=-g-f\cos\omega t$ the effective gravity [33]. The base state is a quiescent fluid with a pressure distribution $p=\rho g_z(t)z$. We absorb the body force in the pressure, so that in what follows p is the deviation from $\rho g_z(t)z$. By applying $-(\boldsymbol{\nabla}\times\boldsymbol{\nabla}\times)$ to Eq. (3), one can eliminate the pressure term, and also obtain a system of equations for the velocity components of $\mathbf{u}=(u,v,w)$, in which the linear terms are uncoupled,

$$\partial_t\nabla^2\mathbf{u}-\nu\nabla^2\nabla^2\mathbf{u}=\boldsymbol{\nabla}\times\boldsymbol{\nabla}\times(\mathbf{u}\cdot\boldsymbol{\nabla})\mathbf{u}. \tag{4}$$

Continuity, $\boldsymbol{\nabla}\cdot\mathbf{u}=0$, has also been used to derive Eq. (4).

Besides the null conditions at $z=-\infty$, there are four boundary conditions at the moving free surface [34]. Let $z=\zeta(x,y)$ be the position of the surface (Fig. 1), then the outward pointing unit normal $\hat{\mathbf{n}}$ is

$$\hat{\mathbf{n}}=\frac{(-\partial_x\zeta,-\partial_y\zeta,1)}{[1+(\partial_x\zeta)^2+(\partial_y\zeta)^2]^{1/2}}. \tag{5}$$

Two linearly independent tangential unit vectors $\hat{\mathbf{t}}_1$ and $\hat{\mathbf{t}}_2$ are

$$\hat{\mathbf{t}}_1=\frac{(1,0,\partial_x\zeta)}{[1+(\partial_x\zeta)^2]^{1/2}},\quad \hat{\mathbf{t}}_2=\frac{(0,1,\partial_y\zeta)}{[1+(\partial_y\zeta)^2]^{1/2}}. \tag{6}$$

Note that these two vectors are not mutually orthogonal. The choice is made so that the expressions for $\hat{\mathbf{t}}_1$ and $\hat{\mathbf{t}}_2$ are symmetric in the Cartesian variables x and y.

The kinematic boundary condition is

$$\partial_t\zeta+[\mathbf{u}(z=\zeta)\cdot\boldsymbol{\nabla}_H]\zeta=w(z=\zeta),$$

with $\boldsymbol{\nabla}_H=\hat{\mathbf{e}}_x\partial_x+\hat{\mathbf{e}}_y\partial_y$. Since the governing equations will be expanded and solved order by order, we mention here its Taylor expansion around $z=0$,

$$\partial_t\zeta+[u+\partial_z u\zeta]_{z=0}\partial_x\zeta+[v+\partial_z v\zeta]_{z=0}\partial_y\zeta =[w+\partial_z w\zeta+\tfrac{1}{2}\partial_{zz}w\zeta^2]_{z=0}. \tag{7}$$

Only terms up to third order in the velocity or surface displacement will be required. In order to avoid excessive use of parentheses, we follow the convention in the remainder of the paper that the operator ∂ acts only on the function immediately following it.

Neglecting the effect of the air phase above the fluid, the tangential stress at the free surface is zero,

$$\hat{\mathbf{t}}_m\cdot\mathbf{T}\cdot\hat{\mathbf{n}}|_{z=\zeta}=0,\quad m=1,2$$

with $\mathbf{T}$ the stress tensor of components, $T_{ij}=[-p-\rho g_z(t)z]\delta_{ij}+\rho\nu(\partial_j u_i+\partial_i u_j)$. The normal stress at the fluid surface is balanced by capillarity,

$$\hat{\mathbf{n}}\cdot\mathbf{T}\cdot\hat{\mathbf{n}}|_{z=\zeta}=2H\sigma,$$

where σ is the interfacial tension and $2H$ is the mean curvature of the surface,

$$2H=\{\partial_{xx}\zeta[1+(\partial_y\zeta)^2]+\partial_{yy}\zeta[1+(\partial_x\zeta)^2] -2\partial_x\zeta\,\partial_y\zeta\,\partial_{xy}\zeta\}/[1+(\partial_x\zeta)^2+(\partial_y\zeta)^2]^{3/2}.$$

The linear stability of the fluid layer under vibration was first addressed in the inviscid limit in [24], and later in [35] in the limit of low viscosity. A complete solution of the stability problem for a fluid of arbitrary viscosity has also been given by Kumar and Tuckerman [31], who reformulated it as an eigenvalue equation for the instability threshold, which was then solved numerically. More recently, Müller *et al.* [30] have derived a low viscosity expansion of the governing equations and boundary conditions, and have used it to obtain analytically the stability boundary up to order $\gamma^{3/2}$. Progress has also been achieved in the opposite limit of large viscous dissipation by Cerda and Tirapegui [36], who have also derived an analytic approximation for the instability threshold. We start by briefly reviewing the formulation of [31] leading to a system of equations that define the instability threshold. We then rewrite their eigenvalue equation as an equivalent, implicit expression for the threshold value which we solve by algebraic iteration instead.

The dominant response of the parametrically driven system is subharmonic at a frequency $\omega/2$ [24]. Although the methodology discussed below can also be used to analyze a possible harmonic response, we restrict our analysis to the subharmonic case. To address the linear stability of the fluid surface, we consider the following solutions for the vertical velocity field and surface displacement:

$$w_0=\cos(kx)\sum_{j=1,3,5,\ldots}e^{ji\omega t/2}w_0^j(z)A_j+\text{c.c.},$$
$$\zeta_0=\cos(kx)\sum_{j=1,3,5,\ldots}e^{ji\omega t/2}A_j+\text{c.c.}, \tag{8}$$

where the A_j are complex amplitudes, and we retain all the harmonics of the fundamental mode $e^{i\omega t/2}$. Truncation of the

sums to include the fundamental mode $e^{ji\omega t/2}$ alone is only appropriate for small viscous damping. From Eq. (4), the linearized equation of motion for w_0 is

$$(\partial_t\nabla^2-\nu\nabla^2\nabla^2)w_0=0.$$

Substituting w_0 and ζ_0 from Eq. (8), one finds

$$[\tfrac{1}{2}ji\omega(-k^2+\partial_{zz})-\nu(-k^2+\partial_{zz})^2]w_0^j(z)=0.$$

The solution of this equation is a linear combination of $e^{\pm kz}$ and $e^{\pm q_j z}$, with $q_j^2=k^2+ji\omega/2\nu$. The linearized kinematic and tangential stress boundary conditions are

$$\partial_t\zeta_0-w_0=0,\quad (\nabla_H^2-\partial_{zz})w_0=0. \tag{9}$$

By using the boundary conditions (9) and the null conditions at $z=-\infty$, $w_0^j(z)$ is given by

$$w_0^j(z)=\left(\frac{1}{2}ji\omega+2\nu k^2\right)e^{kz}-2\nu k^2e^{q_jz}.$$

The first term on the right hand side is the irrotational component of the flow, in which we have explicitly separated the inviscid and viscous contributions. The second term in the right hand side is the rotational component (this is the component that has been neglected in earlier work [22,23]). The linearized normal stress boundary condition is, after having eliminated the pressure by using the equation of motion,

$$[2\nu\nabla_H^2-(\partial_t-\nu\nabla^2)]\partial_z w_0+\left(g-\frac{\sigma}{\rho}\nabla_H^2+f\cos\omega t\right)\nabla_H^2\zeta_0=0. \tag{10}$$

By substituting the assumed solutions given by Eqs. (8) into this equation, we note that the term $2\nu\nabla_H^2\partial_z w_0$ when acting on the irrotational flow component e^{kz} yields a contribution at low viscosity that scales as ν, whereas the rotational contribution (from e^{q_jz}) scales as $\nu^{3/2}$. The remaining term $(\partial_t-\nu\nabla^2)\partial_z w_0$ is simply equal to $-\omega^2$. Hence it is justified to neglect the rotational flow component in the linear stability analysis at low damping. As we show below, and in agreement with [30], rotational flow contributes terms of order $\nu^{3/2}$ and higher to the value of the driving acceleration at onset. In the analysis that follows, however, we retain the full linear solution.

By equating the coefficients of each harmonic $e^{ji\omega t/2}$ resulting from Eq. (10), Kumar and Tuckerman [31] found

$$H_1A_1-fA_1^*-fA_3=0,\quad H_3A_3-fA_1-fA_5=0,$$
$$H_5A_5-fA_3-fA_7=0,\ldots, \tag{11}$$

with

$$H_j=2\left\{\nu^2[4q_jk^4-k(q_j^2+k^2)^2]-gk^2-\frac{\sigma}{\rho}k^4\right\}\Big/\,k^2.$$

This is a system of equations in the unknowns A_j, function of wave number k, and driving amplitude f. By truncating the system (11) at some particular A_n, it can be solved numerically as an eigenvalue problem, f being the eigenvalue. This is indeed what was done by Kumar and Tuckerman [31]. However, note that after truncation at A_n,

$$A_n=\frac{fA_{n-2}}{H_n},\quad A_{n-2}=\frac{fA_{n-4}}{H_{n-2}-f^2/H_n},\quad \ldots \tag{12}$$

so that the infinite set of equations can be rewritten as

$$\left(H_1-\frac{f^2}{H_3-f^2/H_5-\cdots}\right)A_1-fA_1^*\equiv\overline{H}_1(k,f)A_1-fA_1^*=0. \tag{13}$$

For a given wave number k, its threshold of instability f_k is given implicitly by

$$f_k=|\overline{H}_1(k,f_k)|=\left|H_1-\frac{f_k^2}{H_3-\cdots}\right|. \tag{14}$$

The complex amplitude A_j can then be recursively obtained from Eqs. (12) and (13) up to a real factor. The critical wave number for instability $k_{\rm onset}$ corresponds to the lowest value of f_k, f_0.

It is interesting to consider the limiting behavior of Eq. (14) at low viscosity. First recall that for a semi-infinite inviscid fluid, the dispersion relation for surface waves is [26]

$$\omega_0^2=gk_0+\sigma k_0^3/\rho, \tag{15}$$

with $\omega_0=\omega/2$, and k_0 the wave number. In a fluid of low viscosity we expect $k_{\rm onset}$ to be near k_0. It is then convenient to define dimensionless variables by using $1/\omega_0$ as the time scale, and $1/k_0$ as the length scale. We also define a reduced wave number $\overline{k}=k/k_0$, a viscous damping coefficient $\gamma=2\nu k_0^2/\omega_0$, the gravity wave $G=gk_0/\omega_0^2$, and capillary wave $\Sigma=\sigma k_0^3/\rho\omega_0^2$ contributions to the dispersion relation, and the dimensionless amplitude of the driving acceleration $\Delta=fk_0/4\omega_0^2$. Note that $G+\Sigma=1$ from Eq. (15); $G=1$ corresponds to a pure gravity wave while $G=0$ corresponds to a pure capillary wave. For $\gamma\ll1$, $k_{\rm onset}$ and $\Delta_{\rm onset}$ in Eq. (14) can be expanded as a power series of the damping coefficient γ,

$$\overline{k}_{\rm onset}=1+\frac{1}{3-2G}\gamma^{3/2}+\frac{-7+2G}{(3-2G)^2}\gamma^2+\cdots,$$
$$\Delta_{\rm onset}=\gamma-\frac{1}{2}\gamma^{3/2}+\frac{11-2G}{8(3-2G)}\gamma^{5/2}+\cdots. \tag{16}$$

The first correction term is proportional to $\gamma^{3/2}$, and agrees with a low viscosity expansion of the linearized equations [30]. As an example, we plot in Fig. 2 the value of the threshold, $\Delta_{\rm onset}$, as a function of γ at $G=1/3$. Previous low damping calculations of the standing wave amplitude equation [22,23,1] considered the dominant term $\Delta_{\rm onset}=\gamma$ only. Note, however, that the first correction, $-\frac{1}{2}\gamma^{3/2}$, can be a sizable contribution even for small γ (e.g., a 15% difference at $\gamma=0.1$). As a reference, we note that a similar linear analysis based on an inviscid formulation to which viscosity is added through a dissipation function leads to the damped Mathieu equation,

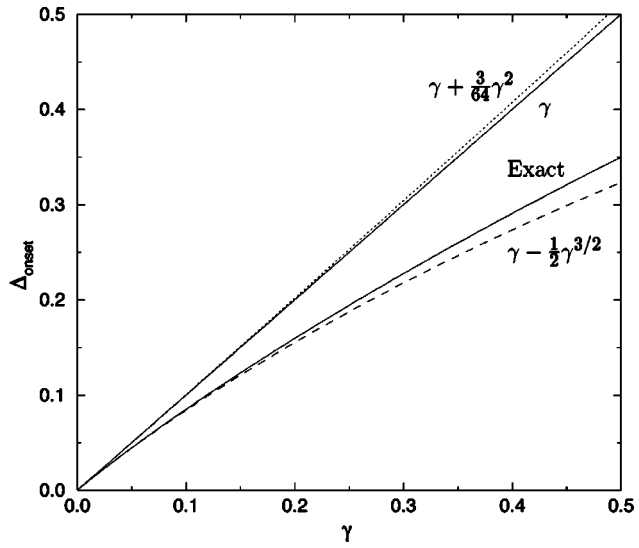

FIG. 2. Dimensionless threshold for linear instability Δ_{onset} as a function of the dimensionless damping parameter γ. The lower solid line is the exact result; the upper solid line is the lowest order approximation in the damping parameter. Also shown are the first order correction in the viscous damping parameter (dashed line), and the first correction for the instability threshold for a damped Mathieu equation (dotted line).

$$\partial_t^2 \hat{\zeta}_k(t) + \gamma \partial_t \hat{\zeta}_k(t) + \omega_0^2 (1 + 2\Delta \cos 2\omega_0 t)\hat{\zeta}_k(t) = 0,$$

where $\hat{\zeta}_k(t)$ is the Fourier transform of $\zeta(x,t)$. This equation gives a threshold at $\gamma + 3\gamma^2/64 + O(\gamma^3)$, which is plotted as the dotted line in Fig. 2. The first correction term is of a different order and has a different sign. Finally, we mention that rotational flow at the linear level in the surface variables can be incorporated exactly as a retarded contribution into the damped Mathieu equation [37].

III. STANDING WAVE AMPLITUDE EQUATION

In this section we use the multiple scale approach [38] to derive a standing wave amplitude equation valid near threshold. As discussed in Sec. I, this approach is based on the assumption that near threshold the wave amplitude evolves in a slow temporal scale. The governing equations and boundary conditions are expanded in a power series of the dimensionless distance away from threshold, ϵ, and solved order by order in ϵ. At the lowest order $[\mathcal{O}(\epsilon^{1/2})]$, we recover the linear problem already discussed in Sec. II, the solution of which yields the surface displacement ζ_0 and the z component of the velocity field w_0. We then compute ζ_1 and w_1, the solutions at $O(\epsilon)$. There is no solvability condition at this order and thus no quadratic terms in the amplitude equation (as dictated by symmetry). The solution at this order, however, is necessary to incorporate triad resonant interactions. At $O(\epsilon^{3/2})$ there appears a solvability condition leading to the desired standing wave amplitude equation.

For a driving amplitude f above threshold, we define $\epsilon = (f - f_0)/f_0$ and expand the flow as

$$\mathbf{u} = \epsilon^{1/2}\mathbf{u}_0 + \epsilon \mathbf{u}_1 + \epsilon^{3/2}\mathbf{u}_2 + \cdots,$$

and similarly for p and ζ. Near threshold, i.e., for $\epsilon \ll 1$, we separate fast and slow time scales: $T = \epsilon t$; $\partial_t \to \partial_t + \epsilon \partial_T$. Spatial slow scales are not included because only regular patterns are considered here. At order $\epsilon^{1/2}$ we recover the linear problem discussed in the preceding section. Since we are interested in standing wave patterns of different symmetries, the solution at this order is written as a linear combination of waves with wave vectors $\mathbf{k}_m$ of magnitude k_{onset} but along different directions in the x-y plane,

$$w_0 = \sum_m \cos(\mathbf{k}_m \cdot \mathbf{x}) B_m(T) \sum_{j=1,3,5,\ldots} e^{ji\omega t/2} w_0^j(z) e_j + \text{c.c.},$$

$$\zeta_0 = \sum_m \cos(\mathbf{k}_m \cdot \mathbf{x}) B_m(T) \sum_{j=1,3,5,\ldots} e^{ji\omega t/2} e_j + \text{c.c.},$$

where $B_m(T)$ are *real* wave amplitudes, functions only of the slow time scale T, and the e_j are the same as the A_j found in Eqs. (12) and (13).

At order ϵ the equation of motion is

$$(\partial_t \nabla^2 - \nu \nabla^2 \nabla^2) w_1 = [\boldsymbol{\nabla} \times \boldsymbol{\nabla} \times (\mathbf{u}_0 \cdot \boldsymbol{\nabla}) \mathbf{u}_0] \cdot \hat{\mathbf{e}}_z. \quad (17)$$

By using the linear solution, the right hand side of Eq. (17) is of the form

$$\sum_{mn}{}' \cos[(\mathbf{k}_m \pm \mathbf{k}_n) \cdot \mathbf{x}] \sum_{j=0,1,2,\ldots} e^{ji\omega t} h_j(z). \quad (18)$$

The first summation is over all possible $\mathbf{k}_m \pm \mathbf{k}_n$, except zero, and the functions $h_j(z)$ are combinations of exponential functions in z that contain the wave amplitudes B_m. Since every term in the right hand side contains a periodic function of $\mathbf{x}$ and exponential functions of t and z, the particular solution of Eq. (17), w_{1p}, can be easily found. The homogeneous solution w_{1h} and ζ_1,

$$w_{1h} = \sum_{mn}{}' \cos[(\mathbf{k}_m \pm \mathbf{k}_n) \cdot \mathbf{x}] \Bigg[\sum_{j=1,2,3,\ldots} e^{ji\omega t} (e^{|\mathbf{k}_m \pm \mathbf{k}_n| z} \alpha_{mn}^{j\pm} + e^{r_{mn}^{j\pm} z} \beta_{mn}^{j\pm}) + \text{c.c.} + e^{|\mathbf{k}_m \pm \mathbf{k}_n| z} \alpha_{mn}^{0\pm} + z e^{|\mathbf{k}_m \pm \mathbf{k}_n| z} \beta_{mn}^{0\pm} \Bigg],$$

$$\zeta_1 = \sum_{mn}{}' \cos[(\mathbf{k}_m \pm \mathbf{k}_n) \cdot \mathbf{x}] \Bigg[\sum_{j=1,2,3,\ldots} e^{ji\omega t} \delta_{mn}^{j\pm} + \text{c.c.} + \delta_{mn}^{0\pm} \Bigg], \quad (19)$$

must now satisfy the boundary conditions. We have defined $(r_{mn}^{j\pm})^2 = |\mathbf{k}_m \pm \mathbf{k}_n|^2 + ji\omega/\nu$. The constants α_{mn}, β_{mn}, and δ_{mn} are determined by the boundary conditions. At this order the boundary conditions are

$$\partial_t \zeta_1 - w_1 = G_{11}(\mathbf{u}_0, \zeta_0),$$

$$(\nabla_H^2 - \partial_{zz}) w_1 = G_{12}(\mathbf{u}_0, \zeta_0),$$

$$(-\partial_t + 3\nu \nabla_H^2 + \nu \partial_{zz}) \partial_z w_1 + \left(g - \frac{\sigma}{\rho} \nabla_H^2 + f_0 \cos \omega t \right) \nabla_H^2 \zeta_1 = G_{13}(\mathbf{u}_0, \zeta_0)$$

where the functions G_{11}, G_{12}, and G_{13} are listed in Appendix A. For each wave vector and harmonic [each m, n, and j in Eq. (19)], the three boundary conditions are sufficient to determine the three unknowns α_{mn}, β_{mn}, and δ_{mn} in Eq. (19). Because the algebra is quite involved (the number of terms is on the order of several thousand), we have in practice used a symbolic manipulation program to solve for these constants.

At order $\epsilon^{3/2}$ the equation of motion becomes

$$(\partial_t\nabla^2-\nu\nabla^2\nabla^2)w_2=-\partial_T\nabla^2 w_0+\{\nabla\times\nabla\times[(\mathbf{u}_0\cdot\nabla)\mathbf{u}_1+(\mathbf{u}_1\cdot\nabla)\mathbf{u}_0]\}\cdot\hat{\mathbf{e}}_z. \tag{20}$$

At this order we only need to consider resonant terms; for example, all terms proportional to $\cos(\mathbf{k}_1\cdot\mathbf{x})$. The right hand side of Eq. (20) is of the form

$$\cos(\mathbf{k}_1\cdot\mathbf{x})\sum_{j=1,3,5,\ldots} e^{ji\omega t/2}E_j(z), \tag{21}$$

where we have used the solutions $(\mathbf{u}_0,\zeta_0,\mathbf{u}_1,\zeta_1)$ already determined. Again, the functions $E_j(z)$ are combinations of exponential functions of their arguments. The solutions for w_2 and ζ_2 are

$$w_2=\cos(\mathbf{k}_1\cdot\mathbf{x})\sum_{j=1,3,5,\ldots} e^{ji\omega t/2}[\overline{E}_j(z)+(a_je^{kz}+b_je^{q_jz})C_j],$$

$$\zeta_2=\cos(\mathbf{k}_1\cdot\mathbf{x})\sum_{j=1,3,5,\ldots} e^{ji\omega t/2}C_j.$$

Here $\overline{E}_j(z)$ is the particular solution that corresponds to the right hand side at this order shown in Eq. (21), and $a_je^{kz}+b_je^{q_jz}$ is the homogeneous solution, which has the same form as the linear solution. We now use the kinematic and tangential stress boundary conditions at this order to determine the constants a_j and b_j, so that the normal stress boundary condition yields a solvability condition for the amplitudes C_j, which in turn leads to the amplitude equations for B_m. The dependence on the wave amplitudes B_m appears through the functions $E_j(z)$, but the functional form is too complicated to be displayed explicitly.

The boundary conditions at this order are

$$\partial_t\zeta_2-w_2=G_{21}(\mathbf{u}_0,\zeta_0,\mathbf{u}_1,\zeta_1),$$

$$(\nabla_H^2-\partial_{zz})w_2=G_{22}(\mathbf{u}_0,\zeta_0,\mathbf{u}_1,\zeta_1),$$

$$(-\partial_t+3\nu\nabla_H^2+\nu\partial_{zz})\partial_z w_2+\left(g-\frac{\sigma}{\rho}\nabla_H^2+f_0\cos\omega t\right)\nabla_H^2\zeta_2=G_{23}(\mathbf{u}_0,\zeta_0,\mathbf{u}_1,\zeta_1),$$

where the functions G_{21}, G_{22}, and G_{23} are listed in Appendix A. By using the first two equations, a_j and b_j are found to satisfy (again with the help of a symbolic manipulation program)

$$a_jC_j=\nu(k^2+q_j^2)C_j+E_j^a,\quad b_jC_j=-2\nu k^2C_j+E_j^b.$$

Here E_j^a and E_j^b are complicated expressions involving the amplitudes of the waves, B_m. Now w_2 and ζ_2 are substituted into the third boundary equation to yield

$$H_1C_1-f_0C_1^*-f_0C_3=F_1,$$

$$H_3C_3-f_0C_1-f_0C_5=F_3,$$

$$H_5C_5-f_0C_3-f_0C_7=F_5,\ldots.$$

The left hand side of this system of equations is identical to Eq. (11) for the linear problem, and the functions F_j on the right hand side are functions of B_m and dB_1/dT. This system of equations can be recast as a single equation in just the same way as in the case of the linear problem,

$$\overline{H}_1C_1-f_0C_1^*=F_1+\frac{f_0}{\overline{H}_3}\left(F_3+\frac{f_0}{\overline{H}_5}(F_5+\cdots)\right)\equiv F, \tag{22}$$

with $\overline{H}_j$ defined similarly to $\overline{H}_1$ in Eq. (13). We now multiply Eq. (22) by $\overline{H}_1^*$ and add the complex conjugate of Eq. (22) multiplied by f_0. By recalling that the threshold of linear instability is given by $f_0=|\overline{H}_1|$, we find

$$F\overline{H}_1^*+F^*f_0=0. \tag{23}$$

This condition plays the role of a solvability condition at this order, and immediately leads to a standing wave amplitude equation for B_1,

$$\frac{dB_1}{dT}=\alpha B_1-g_0B_1^3-\sum_{m\neq 1} g(\theta_{m1})B_m^2B_1, \tag{24}$$

with θ_{m1} the angle between $\mathbf{k}_m$ and $\mathbf{k}_1$. The linear coefficient α (times ϵ) is the linear growth or decay rate of this wave which can be obtained from the linear analysis by adding an extra factor $e^{\alpha t}$ in the definition of w_0 [Eq. (8)]. The coefficient $g(\theta)$ describes the nonlinear interaction between different linearly unstable modes, and provides for the saturation of the wave amplitude.

We first address the dependence of $g(\theta)$ on the damping parameter γ, especially in the limit $\gamma\to 0$. As already discussed in Sec. II, the irrotational and rotational components of the flow contribute to order γ and $\gamma^{3/2}$ to the linear threshold, respectively. Therefore the rotational component of the flow is negligible in the limit of low viscous damping, and it is justified to compute viscous dissipation as if it would arise solely from the irrotational flow. However, the dependence of the nonlinear function $g(\theta)$ on damping is different, as illustrated in Fig. 3 for $g(\theta=90°)$ and $\Sigma=2/3$. As seen in the figure, the contributions to $g(\theta)$ from both the irrotational and rotational flow scale linearly with γ for small γ, and are approximately of the same order of magnitude. This result agrees with the quasipotential approximation [1], and also qualitatively with a recent phenomenological treatment of triad resonance [39].

We next turn to the effect of triad resonant interactions on $g(\theta)$. Figures 4 and 5 show our results for different values of γ and for $\Sigma=0$ (pure gravity waves) and $\Sigma=1/3$ (mixed gravity-capillary waves), respectively. Particular nonlinear

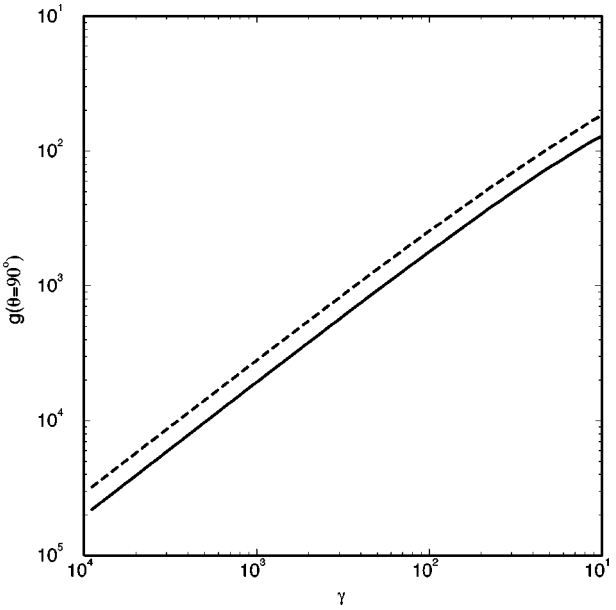

FIG. 3. Nonlinear coefficient $g(\theta=90°)$ at $\Sigma=2/3$. The solid line is the computed value of $g(90°)$, while the dashed line is the same quantity but having kept in the calculation only the irrotational component of the linear solution.

interaction terms that contribute to $g(\theta)$ are shown in Fig. 6. Two linearly unstable modes with wave vectors $\mathbf{k}_m$ and $\mathbf{k}_n$ ($|\mathbf{k}_m|=|\mathbf{k}_n|=k_{\text{onset}}$) interact to produce a wave at $\mathbf{k}_m+\mathbf{k}_n$ with an amplitude proportional to B_mB_n. This mode corresponds to a first order solution [w_1 and ζ_1 in Eqs. (18) and (19)]. Now $\mathbf{k}_m+\mathbf{k}_n$ couples back to the original wave at $-\mathbf{k}_n$ to give a contribution $B_n^2B_m$ to dB_m/dT. Since the mode $\mathbf{k}_m+\mathbf{k}_n$ is damped (only waves with wave numbers near k_{onset} are unstable), this is a dissipative term and contributes to nonlinear saturation of the wave. Triad resonance occurs when the frequency of the mode $\mathbf{k}_m+\mathbf{k}_n$ equals the driving frequency (the modes $\mathbf{k}_m$ and $\mathbf{k}_n$ oscillate at half the driving frequency). Energy is now directly transferred into this mode which can have a very large amplitude at low damping. Since $\mathbf{k}_m+\mathbf{k}_n$ couples back to $-\mathbf{k}_n$, it provides a dissipation channel for the mode $\mathbf{k}_n$. Dissipation is enhanced by triad resonance and results in a large value of $g(\theta_{mn})$ in the vicinity of the resonant angle. The value of the resonant angle can be estimated from the inviscid dispersion relation (15), written in dimensionless form,

$$\overline{\omega^2}=G\overline{k}+\Sigma\overline{k^3}, \tag{25}$$

with $\overline{k}=1$, and $\overline{\omega^2}=G+\Sigma=1$ for the linearly unstable mode. At resonance, we have $\overline{\omega}=2$, and the resonant wave number $\overline{k_r}=|\overline{\mathbf{k}_m}+\overline{\mathbf{k}_n}|$ satisfies $\overline{k_r}(G+\Sigma\overline{k_r^2})=4$. If θ_r is the resonant angle between $\mathbf{k}_m$ and $\mathbf{k}_n$, $\overline{k_r}=\sqrt{2(1+\cos\theta_r)}$, the resonance condition becomes

$$\sqrt{2(1+\cos\theta_r)}[G+2(1+\cos\theta_r)\Sigma]=4. \tag{26}$$

Because $G+\Sigma=1$, this condition can only be satisfied when $\Sigma>1/3$, e.g., $\cos\theta_r=2^{1/3}-1$ for $\Sigma=1$. This result follows entirely from the curvature of the linear dispersion relation for surface waves. Three wave resonant interactions are only possible when the dispersion relation $\omega(k)$ scales as k^λ with $\lambda>1$.

For finite damping, the resonance condition is modified. However, triad resonance is expected to be significant only at low damping because of the damped nature of the first order wave. For example, Fig. 7 shows $g(\theta)$ for different γ and $\Sigma=1$. At small γ, the nonlinear coefficient grows near resonance and peaks at the resonant angle. The value of the peak is seen to decrease with increasing γ. At $\gamma=0.1$, resonance has almost disappeared.

In our calculations presented earlier, resonance arises from the homogeneous solutions w_{1h} and ζ_1, which require finding the constants α_{mn}, β_{mn}, and δ_{mn} in Eq. (19) by enforcing the boundary conditions at first order. The boundary conditions give rise to a system of linear equations for

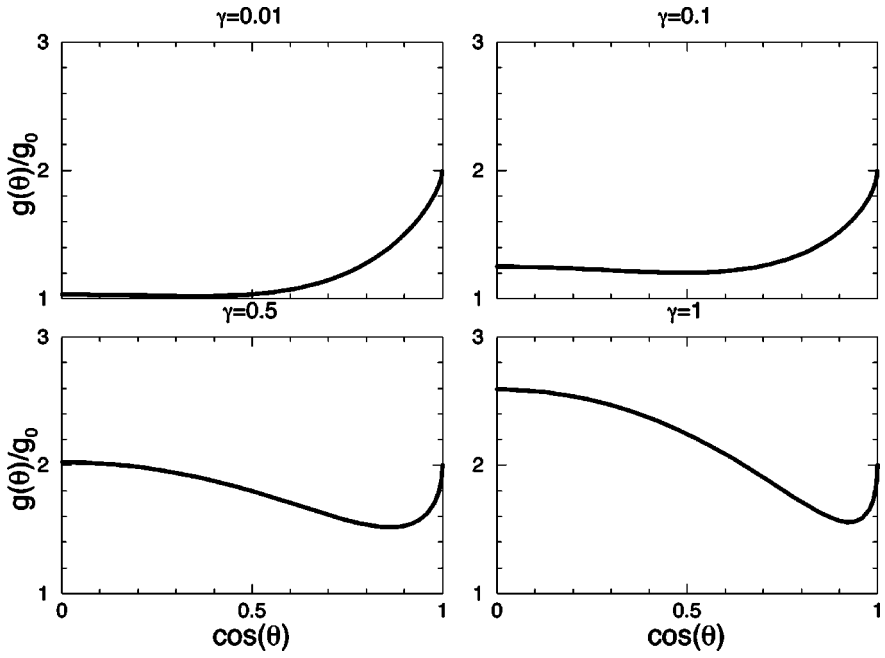

FIG. 4. Cubic term coefficient of the standing wave amplitude equation as a function of angle between wave vectors θ, in the limit of gravity waves, $\Sigma=0$, and different viscous damping coefficients.

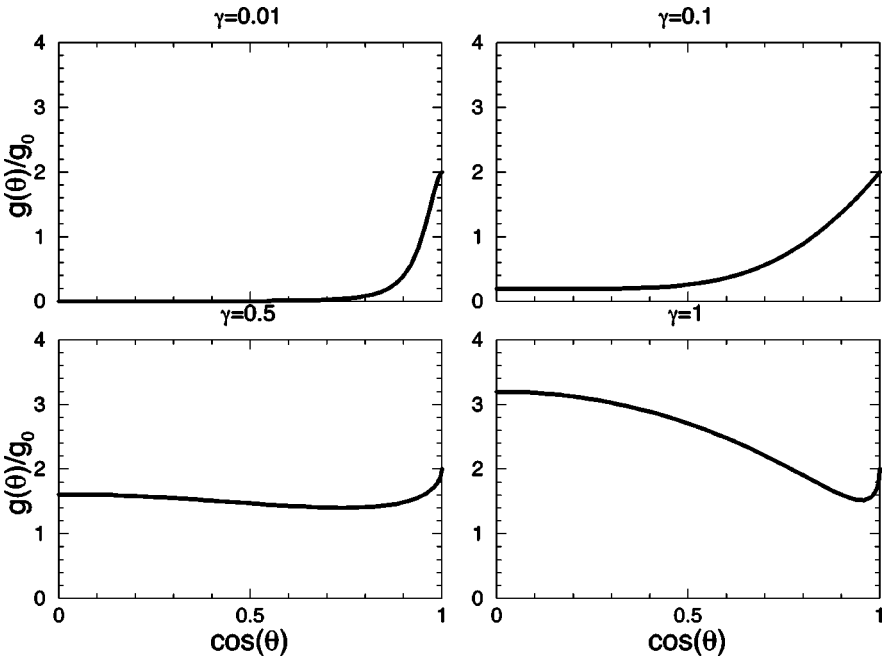

FIG. 5. Cubic term coefficient of the standing wave amplitude equation as a function of angle between wave vectors θ, in the mixed capillary-gravity regime ($\Sigma=1/3$). Note that the curve becomes extremely flat near $\cos\theta=0$ for low γ.

α_{mn}, β_{mn}, and δ_{mn}, the left hand side of which (its matrix form is explicitly given in Appendix B) at $\gamma=0$ has a determinant

$$8\overline{k^2}(G\overline{k^2}+\Sigma\overline{k^4})[4\overline{k}-(G\overline{k^2}+\Sigma\overline{k^4})]^2,$$

which, when equated to zero, is equivalent to Eq. (26).

A particularly noteworthy case corresponds to the region in which the triad resonant angle is close to zero. For the same reasons outlined above, the self-interaction coefficient g_0 now becomes large at small γ. This results in a very small value of $g(\theta)/g_0$ over a wide range of angles for $\Sigma=1/3$ and $\gamma\to 0$, as illustrated in Fig. 5 for $\gamma=0.01$. This peculiar behavior of $g(\theta)$ leads to the appearance of quasiperiodic patterns, as discussed in the following section.

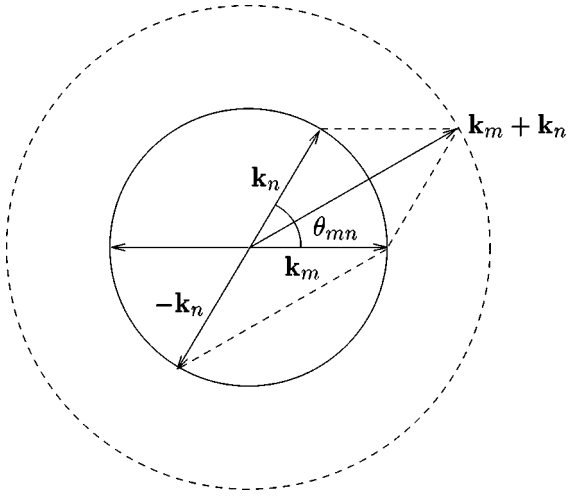

FIG. 6. Schematic representation of a triad resonant interaction: two linearly unstable modes $\mathbf{k}_m$ and $\mathbf{k}_n$ interact to produce a linearly stable mode. This mode interacts with $-\mathbf{k}_n$, leading to resonance with $\mathbf{k}_m$.

IV. PATTERN SELECTION AND COMPARISON WITH EXPERIMENTS

The standing wave amplitude equation (24) can be written in gradient form. Therefore, in principle, the selected pattern near threshold immediately follows [8]. Equation (24) is equivalent to

$$\frac{dB_n}{dT}=-\frac{\delta\mathcal{F}}{\delta B_n},$$

with the Lyapunov function $\mathcal{F}$ given by

$$\mathcal{F}=-\frac{1}{2}\alpha\sum_m B_m^2+\frac{1}{4}\sum_m\sum_n g(\theta_{mn})B_m^2B_n^2,$$

with $g(\theta_{nn})=g_0$ which equals half the value of $g(\theta\to 0)$. The amplitude equation then implies that

$$\frac{d\mathcal{F}}{dT}=\sum_n\frac{\delta\mathcal{F}}{\delta B_n}\frac{dB_n}{dT}=-\sum_n\left(\frac{dB_n}{dT}\right)^2\leqslant 0,$$

so that the preferred pattern can be determined by minimization of $\mathcal{F}$. Such a criterion, however, does not address the stability of the minimizing pattern, nor other experimental complications that may lead to discrepancies between the observed stationary pattern for typical initial conditions and the minimizing pattern. In order to partially address the issue of stability, numerical integration of the governing equations and boundary conditions has been carried out within the quasipotential approximation [40]. Starting from random initial conditions, the asymptotic pattern at long times for a sufficiently large aspect ratio did agree with the theoretical predictions, thus providing indirect evidence of its stability. Other possible effects such as those related to the large coherence length of the pattern near onset at low damping versus the finite size of the experimental system, or to nonvariational effects becoming dominant near onset, have not been addressed. Furthermore, it is also possible that revers-

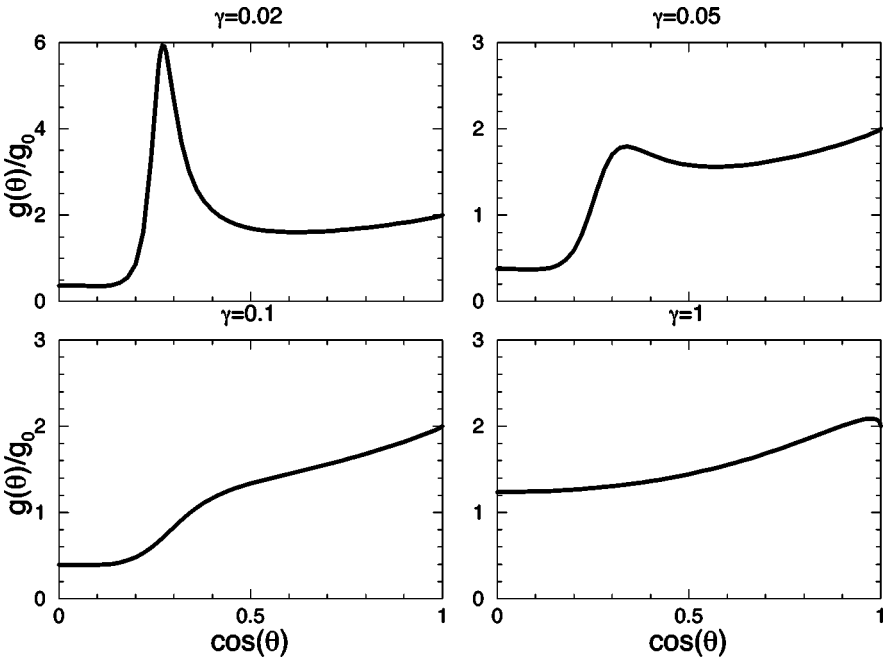

FIG. 7. Cubic term coefficient of the standing wave amplitude equation as a function of angle between wave vectors θ, in the limit of capillary waves, $\Sigma=1$. The large peaks at small values of γ are due to triad resonant interactions.

ible terms of quintic order in the wave amplitude become important at low γ as the cubic coefficient vanishes.

The experimentally observed patterns sufficiently close to threshold are regular patterns consisting of N standing waves, with uniform amplitudes and wave vectors $\mathbf{k}_m$, $m=1,\ldots,N$. The case $N=1$ corresponds to a single standing wave (a pattern of parallel stripes), $N=2$ to a pattern of square symmetry, $N=3$ of hexagonal symmetry, etc. For these regular patterns, the standing wave amplitudes are

$$B_n^2=\frac{\alpha}{g_0+\sum_{m\neq n} g(\theta_{mn})}, \quad n=1,\ldots,N.$$

The value of the Lyapunov function as a function of N then becomes

$$\mathcal{F}(N)=-\frac{\alpha^2}{4}\frac{N}{g_0+\sum_{m=2}^{N} g(\theta_{m1})}. \tag{27}$$

Figure 8 shows the computed values of $\mathcal{F}(N)$ as a function of γ for different values of Σ. For pure gravity waves ($\Sigma=0$), the $N=1$ state has the lowest value of the Lyapunov function and hence will be the selected pattern. At low frequency, the system effectively crosses over to the large

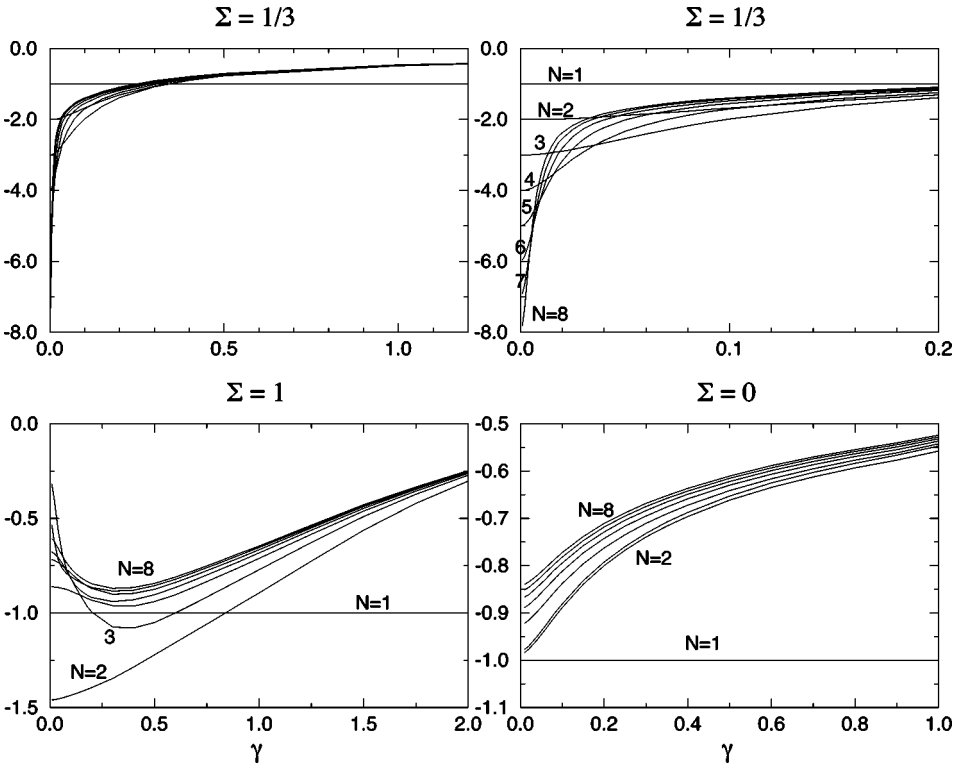

FIG. 8. Numerical values of the Lyapunov function for regular patterns comprising N standing waves as a function of the viscous damping parameter γ. Bottom right: gravity wave limit; bottom left: capillary wave limit; top left, the mixed case of $\Sigma=1/3$; top right is the same as top left but showing the region of small damping in more detail. In the two bottom plots, the curves not labeled are ordered in increasing order of N.

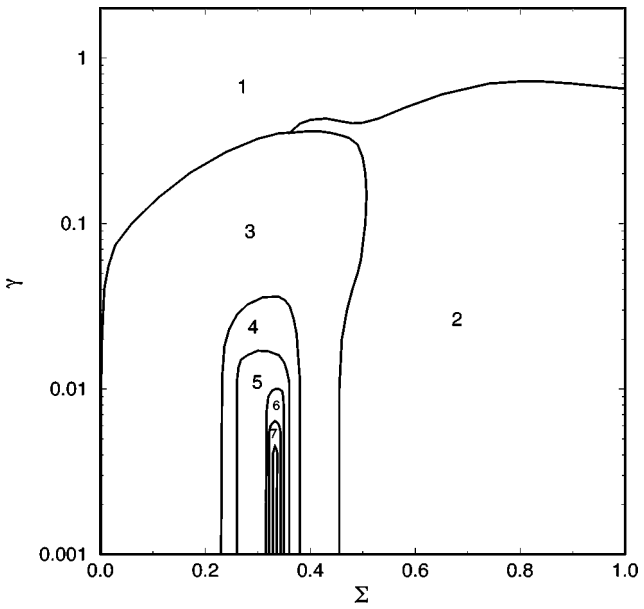

FIG. 9. Selected patterns as a function of γ and Σ. The numbers indicate number of plane waves (1—stripe, 2—square, 3—hexagon, etc.). The smallest region near $\Sigma = 1/3$ should be labeled with an 8.

damping region regardless of its (finite) viscosity (this range was not accessible to our earlier low damping calculation [1]). On the other hand, for pure capillary waves ($\Sigma = 1$) the preferred pattern is $N = 2$ at low damping and $N = 1$ at high damping. Interesting behavior is observed in the vicinity of $\Sigma = 1/3$ (mixed gravity-capillary waves) where the triad resonance angle approaches zero. Hexagonal and higher symmetry quasipatterns are selected with decreasing γ. The low damping results in this region are in qualitative agreement with earlier work [1], although the latter could not account for the transition to $N = 1$ as γ is increased. The appearance of high symmetry patterns is directly attributable to the small value of $g(\theta_{m1})$ compared to g_0 when the triad resonant angle approaches zero. In this region, the value of $\mathcal{F}(N)$ can in fact decrease with increasing the number of wave orientations N. Our results on pattern selection are summarized in Fig. 9. A point worth noting is that although Fig. 8 predicts stripe patterns for all values of γ at $\Sigma = 0$, hexagonal patterns nevertheless persist to very low values of Σ. In fact, the experimental work of Kudrolli and Gollub [2] revealed hexagonal patterns even for the lowest frequencies probed, some of which fall within the region in which we predict an $N = 1$ pattern. As discussed below, we attribute this discrepancy to the shallowness of the fluid layer used in the experiments. We further note that the lines separating regions of square, hexagonal, and quasiperiodic patterns are almost independent of viscosity because they depend mainly on whether the waves are capillarity or gravity dominated, a fact that is largely dependent on the driving frequency and not on viscosity.

We finally compare our predictions [based on Eq. (27)] and two recent sets of experiments that addressed pattern selection in the large aspect ratio limit by Kudrolli and Gollub [2], and by van de Water and collaborators [3,39]. The only input parameters in our calculations are the fluid properties (density, surface tension, and viscosity), and the frequency of the driving acceleration. All these parameters are known fairly precisely in the experimental work, thus allowing a critical comparison between theory and experiments.

TABLE I. Frequencies delimiting regions in which patterns of different symmetries are selected for $\nu = 0.033\,97$ cm^2/s ($\gamma \sim 0.01$–0.03), $\rho = 0.8924$ g/cm^3, and $\sigma = 18.3$ dyn/cm.

Pattern transition	Experiment [3] (Hz)	Theory (Hz)	Weak-damping theory [1] (Hz)
$2 \leftrightarrow 3$	35	35.4	32.8
$3 \leftrightarrow 4$	29	28.7	27.9

Quantitative comparison can be made with the experiments of Binks and van de Water [3], and Binks, Westra, and van de Water [39]. They developed a cell of exceptionally large aspect ratio and used a fluid layer of depth much larger than the wavelength. A summary of their findings, along with our predictions and those of [1] are shown in Table I. The location of the lines separating regions of stability of patterns of square, hexagonal, and eightfold symmetry is in excellent agreement with our predictions. We note that they carefully studied the effect of layer depth on the location of these transition lines [39]. The values given in Table I are their results for the deeper layers when the transition frequency is seen to become independent of layer depth. In this experiment, patterns with $N = 5$ are observed around 27 Hz. We agree with the authors of the experiment that this discrepancy may be due to finite size effects. In fact, $\mathcal{F}(5)$ is very close to $\mathcal{F}(4)$ at about 26 Hz (the difference is less than 0.2%), although $\mathcal{F}(5) > \mathcal{F}(4)$. The table also shows better agreement between the experiments and our theory than with earlier results based on the quasipotential approximation of [1]. A possible explanation for the larger discrepancy involves the fact that they only used the term linear in γ in the calculation of the threshold for instability [Eq. (16)]. Omitting the first correction (of order $\gamma^{3/2}$) yields a similar percentage error in the value of the instability threshold (for γ in the range 0.01–0.03 as is appropriate for this experiment).

The contribution of triad resonant interactions to the cubic coefficient of the amplitude equation and their role on pattern selection have been discussed by Binks *et al.* [39]. By experimentally examining the stability region of patterns of high symmetry as a function of fluid layer depth, they are able to establish the dominant role of triad resonant interactions to dissipation at low damping. Their results are in complete agreement with those presented in this paper. We note that this coupling has been neglected in previous research that built upon inviscid theory.

A recent comprehensive survey of pattern selection involving a wide range of fluid viscosities and driving frequencies has been conducted by Kudrolli and Gollub [2]. They also focused on the large aspect ratio limit although the depth of the fluid layer used in the experiments (0.3 cm) was smaller than the wavelength (1–3 cm). Although their observations are generally in good agreement with our predictions, even quantitatively, it is difficult to draw definite conclusions until the influence of layer depth on the observed patterns is understood. Their findings, summarized in Table I of their paper, are as follows: hexagonal patterns at low frequency for all viscosities, square patterns at high frequency and low

viscosity, and stripe patterns at high viscosity. These observations are in agreement with our predictions (Fig. 9). The measured transition boundaries are also quite close to our predictions [5]. However, they did not observe quasipatterns in the region predicted by our theory. This lack of quasipatterns is now understood to be a consequence of the small fluid layer depth [39].

Additional experimental work has been conducted in the range of large driving frequency [15,41]. Up to frequencies of 350 Hz, both experiments show a bifurcation to square patterns, in agreement with our predictions. At higher frequencies, the experiments of Christiansen *et al.* [15] bifurcated to eightfold quasipatterns, in disagreement with our theory.

In summary, we have presented a nonlinear theory for Faraday waves in viscous fluids with no assumptions or approximations other than those inherent to the multiscale expansion. A set of standing wave amplitude equations has been obtained that is of gradient form. Minimization of the associated Lyapunov function leads to determination of the preferred pattern near threshold. The predicted patterns are in excellent agreement with recent experiments in large aspect ratio systems involving a range of fluid viscosities and driving frequencies. According to Fig. 9, the transition from square to stripe patterns remains in the capillary wave limit of $\Sigma=1$ (high frequency limit in the experiments). At low Σ (low frequency limit in the experiments) there is a transition from hexagons to stripes, although only stripes are selected around $\Sigma=0$. Furthermore, all the high symmetry patterns (with $N\geqslant 3$) are observed in the vicinity of $\Sigma=1/3$, the point at which the triad resonant angle approaches zero, and for low damping where the resonance is more pronounced.

ACKNOWLEDGMENTS

This research has been supported by the U.S. Department of Energy under Contract No. DE-FG05-95ER14566, and also in part by the Supercomputer Computations Research Institute, which is partially funded by the U.S. Department of Energy under Contract No. DE-FC05-85ER25000.

APPENDIX A: INHOMOGENEOUS TERMS OF THE FIRST AND SECOND ORDER EQUATIONS

We list in this appendix the functions G_{ij}, the inhomogeneous terms in the boundary conditions at first and second order.

$$G_{11}=\partial_z w_0\zeta_0-u_0\partial_x\zeta_0-v_0\partial_y\zeta_0,$$

$$\begin{aligned}G_{12}=&\partial_x[-\partial_{zz}u_0\zeta_0-\partial_{xz}w_0\zeta_0+2(\partial_x u_0-\partial_z w_0)\partial_x\zeta_0+(\partial_y u_0+\partial_x v_0)\partial_y\zeta_0]\\&+\partial_y[-\partial_{zz}v_0\zeta_0-\partial_{yz}w_0\zeta_0+2(\partial_y v_0-\partial_z w_0)\partial_y\zeta_0+(\partial_x v_0+\partial_y u_0)\partial_x\zeta_0],\end{aligned}$$

$$G_{13}=-\rho\nabla_H\cdot[(\mathbf{u}_0\cdot\nabla)\mathbf{u}_0]+\nabla_H^2(-2\eta\partial_{zz}w_0\zeta_0+\partial_z p_0\zeta_0),$$

$$G_{21}=-\partial_T\zeta_0-u_0\partial_x\zeta_1-u_1\partial_x\zeta_0-\partial_z u_0\zeta_0\partial_x\zeta_0-v_0\partial_y\zeta_1-v_1\partial_y\zeta_0-\partial_z v_0\zeta_0\partial_y\zeta_0+\partial_z w_0\zeta_1+\partial_z w_1\zeta_0+\tfrac{1}{2}\partial_{zz}w_0\zeta_0^2,$$

$$\begin{aligned}G_{22}=&\partial_x[-\partial_{zz}u_1\zeta_0-\partial_{zz}u_0\zeta_1-\tfrac{1}{2}\partial_{zzz}u_0\zeta_0^2-\partial_{xz}w_1\zeta_0-\partial_{xz}w_0\zeta_1-\tfrac{1}{2}\partial_{xzz}w_0\zeta_0^2-2(\partial_z w_1-\partial_x u_1)\partial_x\zeta_0-2(\partial_z w_0-\partial_x u_0)\partial_x\zeta_1\\&-2\partial_z(\partial_z w_0-\partial_x u_0)\zeta_0\partial_x\zeta_0+(\partial_y u_1+\partial_x v_1)\partial_y\zeta_0+(\partial_y u_0+\partial_x v_0)\partial_y\zeta_1+\partial_z(\partial_y u_0+\partial_x v_0)\zeta_0\partial_y\zeta_0]\\&+\partial_y[-\partial_{zz}v_1\zeta_0-\partial_{zz}v_0\zeta_1-\tfrac{1}{2}\partial_{zzz}v_0\zeta_0^2-\partial_{yz}w_1\zeta_0-\partial_{yz}w_0\zeta_1-\tfrac{1}{2}\partial_{yzz}w_0\zeta_0^2-2(\partial_z w_1-\partial_y v_1)\partial_y\zeta_0-2(\partial_z w_0-\partial_y v_0)\partial_y\zeta_1\\&-2\partial_z(\partial_z w_0-\partial_y v_0)\zeta_0\partial_y\zeta_0+(\partial_y u_1+\partial_x v_1)\partial_x\zeta_0+(\partial_y u_0+\partial_x v_0)\partial_x\zeta_1+\partial_z(\partial_y u_0+\partial_x v_0)\zeta_0\partial_x\zeta_0],\end{aligned}$$

$$\begin{aligned}G_{23}=&-\rho\nabla_H\cdot[(\mathbf{u}_0\cdot\nabla)\mathbf{u}_1+(\mathbf{u}_1\cdot\nabla\mathbf{u}_0)]+\rho\partial_T\partial_z w_0+\nabla_H^2[-\tfrac{1}{2}\rho f_0(e^{i\omega t}+e^{-i\omega t})\zeta_0+\partial_z p_1\zeta_0+\partial_z p_0\zeta_1+\tfrac{1}{2}\partial_z^2 p_0\zeta_0^2\\&-2\eta\partial_z^2 w_1\zeta_0-2\eta\partial_z^2 w_0\zeta_1-\eta\partial_z^3 w_0\zeta_0^2+2\eta(\partial_z u_1+\partial_x w_1)\partial_x\zeta_0+2\eta(\partial_z w_0-\partial_x u_0)(\partial_x\zeta_0)^2\\&+2\eta(\partial_z v_1+\partial_y w_1)\partial_y\zeta_0+2\eta(\partial_z w_0-\partial_y v_0)(\partial_y\zeta_0)^2-2\eta(\partial_y u_0+\partial_x v_0)\partial_x\zeta_0\partial_y\zeta_0-\tfrac{3}{2}\sigma\partial_{xx}\zeta_0(\partial_x\zeta_0)^2\\&-\tfrac{3}{2}\sigma\partial_{yy}\zeta_0(\partial_y\zeta_0)^2-\tfrac{1}{2}\sigma\partial_{xx}\zeta_0(\partial_y\zeta_0)^2-\tfrac{1}{2}\sigma\partial_{yy}\zeta_0(\partial_x\zeta_0)^2-2\sigma\partial_x\zeta_0\partial_y\zeta_0\partial_{xy}\zeta_0].\end{aligned}$$

APPENDIX B: MATRIX OF COEFFICIENTS AT FIRST ORDER

Left hand side of the system of linear equations for the first order solution (for simplicity, we only show the case $\gamma\ll 1$ and the coefficients of first time harmonic $e^{i\omega t/2}$),

$$\begin{pmatrix} -1 & 0 & 0 & -1 & 0 & 0 & -2i & 0 & 0 \\ 0 & -1 & 0 & 0 & -1 & 0 & 0 & 0 & 0 \\ 0 & 0 & -1 & 0 & 0 & -1 & 0 & 0 & 2i \\ -\gamma\overline{k^2} & 0 & 0 & 2i & 0 & 0 & 0 & 0 & 0 \\ 0 & -\overline{k^2} & 0 & 0 & -\overline{k^2} & 0 & 0 & 0 & 0 \\ 0 & 0 & -\gamma\overline{k^2} & 0 & 0 & -2i & 0 & 0 & 0 \\ -2i\overline{k} & 0 & 0 & \gamma\overline{k^2}\,\overline{q}^* & 0 & 0 & G\overline{k^2}+\Sigma\overline{k^4} & 2\gamma\overline{k^2} & 0 \\ 0 & \gamma\overline{k^3} & 0 & 0 & 0 & 0 & 2\gamma\overline{k^2} & G\overline{k^2}+\Sigma\overline{k^4} & 2\gamma\overline{k^2} \\ 0 & 0 & 2i\overline{k} & 0 & 0 & \gamma\overline{k^2}\,\overline{q} & 0 & 2\gamma\overline{k^2} & G\overline{k^2}+\Sigma\overline{k^4} \end{pmatrix} \begin{pmatrix} \alpha_{mn}^{1-} \\ \alpha_{mn}^{0} \\ \alpha_{mn}^{1+} \\ \beta_{mn}^{1-} \\ \beta_{mn}^{0} \\ \beta_{mn}^{1+} \\ \delta_{mn}^{1-} \\ \delta_{mn}^{0} \\ \delta_{mn}^{1+} \end{pmatrix},$$

with $\overline{k}=|\overline{\mathbf{k}}_m+\overline{\mathbf{k}}_n|$ and $\overline{q^2}\equiv\overline{k^2}+2i/\gamma$.

[1] W. Zhang and J. Viñals, J. Fluid Mech. **336**, 301 (1997).
[2] A. Kudrolli and J. Gollub, Physica D **97**, 133 (1996).
[3] D. Binks and W. van de Water, Phys. Rev. Lett. **78**, 4043 (1997).
[4] W. Zhang and J. Viñals, Phys. Rev. E **53**, R4283 (1996).
[5] P. Chen and J. Viñals, Phys. Rev. Lett. **79**, 2670 (1997).
[6] M. Faraday, Philos. Trans. R. Soc. London **121**, 319 (1831).
[7] J. Miles and D. Henderson, Annu. Rev. Fluid Mech. **22**, 143 (1990).
[8] M. Cross and P. Hohenberg, Rev. Mod. Phys. **65**, 851 (1993).
[9] W. Edwards and S. Fauve, J. Fluid Mech. **278**, 123 (1994).
[10] L. Daudet, V. Ego, S. Manneville, and J. Bechhoefer, Europhys. Lett. **32**, 313 (1995).
[11] R. Lang, J. Acoust. Soc. Am. **34**, 6 (1962).
[12] A. Ezerskii, M. Rabinovich, V. Reutov, and I. Starobinets, Zh. Éksp. Teor. Fiz. **91**, 2070 (1986) [Sov. Phys. JETP **64**, 1228 (1986)].
[13] N. Tufillaro, R. Ramshankar, and J. Gollub, Phys. Rev. Lett. **62**, 422 (1989).
[14] S. Ciliberto, S. Douady, and S. Fauve, Europhys. Lett. **15**, 23 (1991).
[15] B. Christiansen, P. Alstrøm, and M. Levinsen, Phys. Rev. Lett. **68**, 2157 (1992).
[16] H. Müller, Phys. Rev. Lett. **71**, 3287 (1993).
[17] K. Kumar and K. Bajaj, Phys. Rev. E **52**, R4606 (1995).
[18] H. Müller, Phys. Rev. E **49**, 1273 (1994).
[19] V. Zakharov, Prikl. Mekh. Tekh. Fiz. **9**, 86 (1968) [J. Appl. Mech. Tech. Phys. **9**, 190 (1968)].
[20] J. Miles, J. Fluid Mech. **83**, 153 (1977).
[21] J. Miles, J. Fluid Mech. **146**, 285 (1984).
[22] S. Milner, J. Fluid Mech. **225**, 81 (1991).
[23] J. Miles, J. Fluid Mech. **248**, 671 (1993).
[24] T. Benjamin and F. Ursell, Proc. R. Soc. London, Ser. A **225**, 505 (1954).
[25] P. Coullet, T. Frisch, and G. Sonnino, Phys. Rev. E **49**, 2087 (1994).
[26] L. Landau and E. Lifshitz, *Fluid Mechanics* (Pergamon, New York, 1959).
[27] P. Hansen and P. Alstrøm, J. Fluid Mech. **351**, 301 (1997).
[28] The governing equations are invariant under time translation by a period of the driving force $t\rightarrow t+2\pi/\omega$. Subharmonic response implies that $\zeta(x,y,t+2\pi/\omega)=-\zeta(x,y,t)$, with $z=\zeta(x,y,t)$ the position of the surface. Because of this invariance, the amplitude equation for A_j must also be invariant under a sign change in A_j.
[29] T. Lundgren and N. Mansour, J. Fluid Mech. **194**, 479 (1988).
[30] H. Müller *et al.*, Phys. Rev. Lett. **78**, 2357 (1997).
[31] K. Kumar and L. Tuckerman, J. Fluid Mech. **279**, 49 (1994).
[32] K. Kumar, Proc. R. Soc. London, Ser. A **452**, 1113 (1996).
[33] We use a driving acceleration proportional to $\cos\omega t$ instead of $\sin\omega t$ as in [1] to avoid, as discussed in that reference, the complication related to the parity under time reversal of the driving acceleration.
[34] H. Lamb, *Hydrodynamics*, 6th ed. (Dover, New York, 1945).
[35] L. Landau and E. Lifshitz, *Mechanics* (Pergamon, New York, 1976).
[36] E. Cerda and E. Tirapegui, Phys. Rev. Lett. **78**, 859 (1997).
[37] Nam Hong U, Bull. Russ. Acad. Sci. Phys. Suppl. **57**, 131 (1993).
[38] A. Newell and J. Whitehead, J. Fluid Mech. **38**, 279 (1969).
[39] D. Binks, M.-T. Westra, and W. van de Water, Phys. Rev. Lett. **79**, 5010 (1997).
[40] W. Zhang and J. Viñals, Physica D **116**, 225 (1998).
[41] E. Bosch and W. van de Water, Phys. Rev. Lett. **70**, 3420 (1993).